The Astrophysical Journal, 809:139 (13pp), 2015 August 20 doi:10.1088/0004-637X/809/2/139

MODELING INDICATIONS OF TECHNOLOGY IN PLANETARY TRANSIT LIGHT CURVES—DARK-SIDE ILLUMINATION

Eric J. Korpela[1], Shauna M. Sallmen[2], and Diana Leystra Greene[2]
[1] Space Sciences Laboratory, University of California at Berkeley, Berkeley, CA, 94720, USA; korpela@ssl.berkeley.edu
[2] University of Wisconsin—La Crosse, La Crosse, WI 54601, USA
Received 2014 September 13; accepted 2015 July 14; published 2015 August 18

ABSTRACT

We analyze potential effects of an extraterrestrial civilization's use of orbiting mirrors to illuminate the dark side of a synchronously rotating planet on planetary transit light curves. Previous efforts to detect civilizations based on side effects of planetary-scale engineering have focused on structures affecting the host star output (e.g., Dyson spheres). However, younger civilizations are likely to be less advanced in their engineering efforts, yet still capable of sending small spacecraft into orbit. Since M dwarfs are the most common type of star in the solar neighborhood, it seems plausible that many of the nearest habitable planets orbit dim, low-mass M stars, and will be in synchronous rotation. Logically, a civilization evolving on such a planet may be inspired to illuminate their planet's dark side by placing a single large mirror at the L2 Lagrangian point, or launching a fleet of small thin mirrors into planetary orbit. We briefly examine the requirements and engineering challenges of such a collection of orbiting mirrors, then explore their impact on transit light curves. We incorporate stellar limb darkening and model a simplistic mirror fleet's effects for transits of Earth-like ($R = 0.5$ to 2 $R_{\rm Earth}$) planets which would be synchronously rotating for orbits within the habitable zone of their host star. Although such an installation is undetectable in *Kepler* data, the *James Webb Space Telescope* will provide the sensitivity necessary to detect a fleet of mirrors orbiting Earth-like habitable planets around nearby stars.

Key words: astrobiology – extraterrestrial intelligence – planets and satellites: terrestrial planets

1. INTRODUCTION

The detection by *Kepler* (Petigura et al. 2013; Marcy et al. 2014) of multiple Earth-like planets in or near the habitable zones (HZs) of late-type stars has renewed interest in the search for extraterrestrial intelligence (SETI). Most prior searches concentrated on detecting electromagnetic communications in radio/microwaves and optical/IR bands (Sagan & Drake 1975; Bowyer et al. 1997; Tarter 2001; Howard et al. 2007; Korpela et al. 2011; Von Korff et al. 2013). Such searches have operated intermittently since the 1960 s and continue today with greatly enhanced frequency coverage and detection sensitivity.

Freitas (1983) suggested that the first evidence we find of an extraterrestrial civilization may be the detection of a physical artifact rather than an electromagnetic signal. In this paper, we investigate the potential for detection of a large fleet of small spacecraft in orbit around a terrestrial exoplanet, for example, mirrors illuminating the dark side of a planet in synchronous rotation. Such a fleet could be observable through its effect on the transit light curve.

The remainder of the introduction motivates this scenario and places it in context with conjectures regarding other extraterrestrial engineering projects and our current understanding of exoplanet habitability. In Section 2.1, we explore plausible methods of dark-side illumination, discussing associated technical and engineering challenges in Section 2.2. Section 3 describes a simple model of the effects of an orbiting mirror fleet on transit light curves. We present the resulting light curves in Section 4, focusing on the signature and magnitude of the mirrors' influence, and examining the effects of altering various stellar, planetary, and mirror fleet parameters. We consider prospects for detection in Section 5.

1.1. Motivation

The most common type of star in our Galaxy is the M dwarf. These stars have very long lives. Because of their low luminosity, the HZ around M dwarfs is narrow and close to the star. Due to tidal considerations, such planets will probably always present one face to the star, except in unusual cases. (Tarter et al. 2007). Although young (<100 Myr) dM stars have active chromospheres and high UV output that could be damaging to biological organisms, such activity decreases rapidly with age (Engle et al. 2009). There is also a wide variation in activity at all ages (Shkolnik & Barman 2014), and its precise impact on exoplanet atmospheres, water content, magnetospheres, and habitability is a subject of active research (e.g., Grenfell et al. 2012; Zuluaga et al. 2013; Mulders et al. 2014; Tian 2014). Since the specific conditions required for the evolution of an ecosystem are not well-defined, and given that M and K dwarfs are 80% of stars in the solar neighborhood (Henry et al. 2006), it seems plausible that most nearby habitable planets are in synchronous rotation in orbits around low-mass stars. A significant fraction of M dwarfs do host small planets within their HZs, with the detailed estimates depending on the choice of HZ (Dressing & Charbonneau 2013; Gaidos 2013; Kopparapu 2013).

Life around an M dwarf could pose unique challenges for life and for the evolution of intelligence. However, once a civilization has either evolved *in planeta* or migrated from elsewhere, it might wish to utilize portions of the planet that do not receive illumination from the star. After careful consideration of the climatic effects, the first deliberate planetary scale engineering project might be the illumination of the planet's dark side. The most straightforward method is via orbiting thin mirrors, either placing a single large mirror at the L2 Lagrange point or, more likely, launching a fleet of smaller mirrors into lower orbits. To provide significant illumination, these mirrors

must have a total reflective surface area approximately equal to the disk area of the planet. This could render them detectable in a planetary transit.

If the primary motivation is dark-side illumination, we anticipate such structures would be found primarily around synchronously rotating planets, most likely orbiting M stars. As we discuss in Section 3.1, habitable worlds in certain orbits around earlier-type stars (e.g., G stars) might also be in synchronous rotation at the current time. In addition, an alien civilization might wish to utilize a previously uninhabited planet in their star system, or simply ensure illumination of the night side of a planet in non-synchronous rotation. Other possible uses of fleets of comparable area include photoelectric power generation. Thus, although in what follows we focus our attention on worlds with a perpetual dark side, such engineering projects might occur in other situations, and around many types of stars.

1.2. Prior Proposed Megastructures

Dyson (1960) suggested that an extraterrestrial civilization might build a giant structure to capture and utilize most or all of the visible emissions of a star, radiating only waste heat. A Dyson sphere would be detectable as a stellar-luminosity ~300 K featureless blackbody source if the structure completely encases the star, or as a star with a significant infrared (IR) excess in the case of a partial sphere. If civilizations capable of such feats of engineering were common, we could likely detect them in IR surveys. Searches of the IR sky sensitive to both complete (Carrigan 2009) and partial (Jugaku & Nishimura 2004; Conroy & Werthimer 2003, unpublished;[3] Globus et al. 2003, unpublished[4]). Dyson spheres have been conducted using the *IRAS* data set. While these have detected a few interesting candidates, none have been shown to indicate intelligent origin. Two high-sensitivity searches for Dyson spheres are ongoing, one searching for IR signatures of Dyson spheres in the *WISE* survey (Wright et al. 2014b, 2014a; Griffith et al. 2015), and another examining *Kepler* light curves for unusual transit eclipses that could indicate a partial Dyson sphere (Marcy et al. 2013).

A civilization advanced enough to trap most of the available output of their host star ($\sim 4 \times 10^{33}$ erg s^{-1}) meets the definition of Kardashev Type II on Kardashev's (1964) scale of technological advancement of a civilization. A Type I civilization uses energy on the scale of current terrestrial civilization ($\sim 4 \times 10^{19}$ erg s^{-1}). Given the possibility of extinction, it seems likely that Kardashev Type II civilizations are much rarer than those capable of sending small spacecraft into orbit and that a continuum of possible engineering stages should exist. We might consider a civilization with significant ability to modify its planetary environment, but not capable of building AU scale structures as Type I.5.

Carrigan (2012) recently summarized several other potential archaeological signatures for civilizations at various levels on the Kardashev scale, concluding that, apart from electromagnetic communications, these are generally undetectable with current human technologies. Arnold (2005) suggests that an extraterrestrial civilization could deliberately create planetary scale structures with unique shapes or periodicities that could be detected when the structure transits the star, but could be distinguished from a planetary transit with current technology. Our proposed engineering project is of a similar scale, but with a useful function besides communication and with a form that follows from its function.

[3] From http://seti.berkeley.edu/IR_Excess_Search retrieved 2015 July 09.
[4] Mentioned in Carrigan (2009).

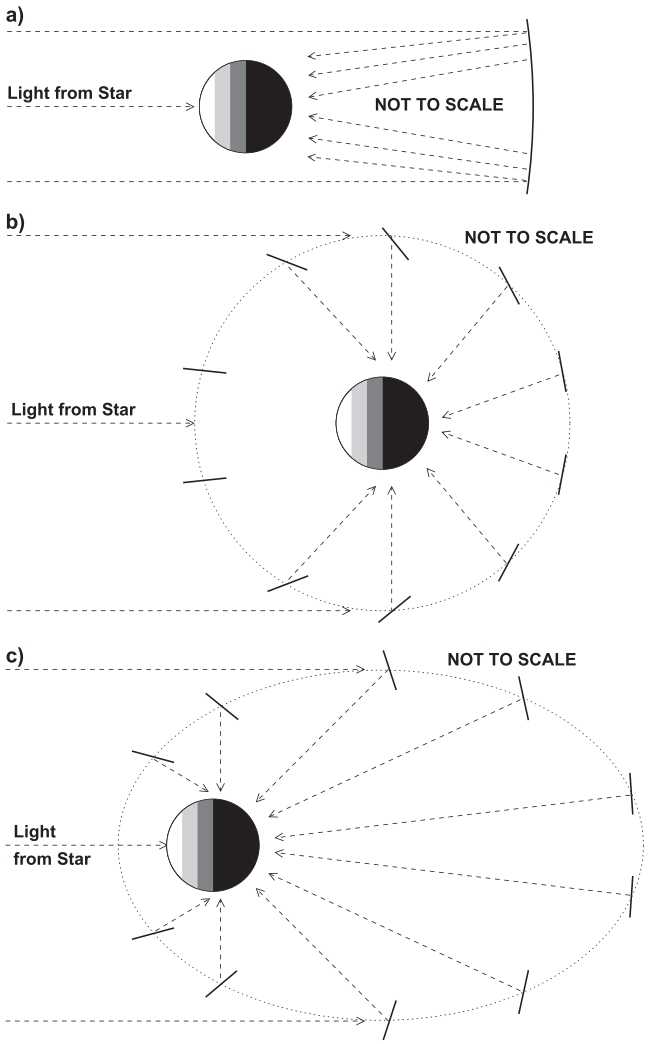

Figure 1. Schematic illustration of three methods of dark-side illumination (not to scale). Planetary grayscale bands indicate different levels in stellar illumination. In the three cross-sectional drawings, (a) shows a large circular or annular mirror stationed at the L2 Lagrange point, (b) shows multiple small mirrors in circular orbits, (c) shows multiple small mirrors in elliptical orbits designed to maximize the duty cycle of the mirrors.

2. DARK-SIDE ILLUMINATION UTILIZING MIRRORS

2.1. Methods of Dark-side Illumination

There are multiple methods by which an alien civilization could illuminate the dark side of a synchronously rotating planet. Conceptually, the simplest is placing a single large mirror at the L2 Lagrange point (Figure 1(a)). To provide illumination equivalent to the bright-side stellar illumination, it would need to be a large disk or annulus somewhat larger than the planetary diameter. Since the mirror is locked in the anti-stellar direction it would provide non-uniform directional illumination on the ground, with regions near the terminator receiving illumination at higher incidence angles than regions near the anti-stellar point. One notable difficulty is maintaining positional and directional stability at the unstable L2 point. A

structure and control system that could allow pointing and positional control of a 6000–25000 km diameter mirror would be a significant engineering challenge.

In the case of a single large ($R_m > R_p$) mirror at the L2 Lagrange point, the optical transit light curve will last longer and be deeper than if only the planet blocked the starlight. If the mirror has been engineered so all intercepted light is redirected to the planet, and none toward our line of sight, the planetary eclipse phase will be the same as if the mirror were not present. Thus the difference in transit and eclipse time span would be the main clue to the presence of such a structure, but a similar timing effect could occur for a planet in a highly elliptical orbit with periastron at the time of eclipse and apastron at the time of transit.

A less technically challenging method would be to deploy a fleet of independently steerable smaller mirrors. Figure 1(b) schematically illustrates this possibility in cross-section for mirrors in a circular orbit. Elongated mirror orbits, as depicted in Figure 1(c), might be preferable, since they spend a greater fraction of their orbital period in a position to usefully illuminate the planet's dark side.

For a fleet of many individual reflectors, the translucent fleet of mirrors would block some starlight, deepening and lengthening the transit. Before modeling in detail the effects of a fleet of space-based mirrors on transit light curves, we first discuss technical and engineering considerations involved in its implementation.

2.2. Technical and Engineering Considerations

Current materials technologies allow for the construction of metalized plastic films with surface mass densities of 0.7–1.5 mg cm^{-2}; neglecting supporting structures, the mass of a 1 km^2 mirror would be 7000–15000 kg (Bryant et al. 2014). Future materials development (carbon nanotube fabrics: Lima et al. 2011, space-based fabrication of metal films: Wright 1992) could result in materials with surface mass densities from 0.01mg cm^{-2} to as little as 0.002mg cm^{-2}. This provides the potential to allow in situ creation of 1 km^2 reflective surfaces with masses of 20–100 kg. For these, structure and propulsion/control systems will likely be the dominant mass. Each reflector could be pointed based upon orbital position, and controlled independently and autonomously.

We will not attempt a detailed discussion of the dynamics of such an installation in this paper. However, we can utilize the planet's L2 Lagrangian point to estimate the largest stable orbits in the effective planetary gravitational well. For a planet in orbit at the inner edge of the HZ of an M8 star (as estimated below in Section 3.1), the Lagrange point is beyond 10 planetary radii, and is even more distant for earlier stellar types. Therefore, for mirror flotillas with orbits of modest extent ($\lesssim$5 planetary radii), the mirror orbits should be relatively stable and controllable.

Providing a reflective area equivalent to Earth's disk area (1.3×10^8 km^2) requires deployment of more than 130 million mirrors of 1 km^2 each, or 1.3 million mirrors of 100 km^2. At 1000 kg km^{-2} even a 100 km^2 reflector lies within current human launch capabilities. However, even with optimistic ($2200 kg^{-1}) estimates,[5] launch costs for such a fleet exceed $\$2.8 \times 10^{16}\mathrm{USD}_{2015}$.

There will undoubtedly be significant environmental impacts due to pollution from manufacturing, launch exhaust products, and altering the energy balance of the planet. However, we leave the details of engineering a climatic balance, combating pollution, and the possible sacrifice of a millennium of economic output to the inhabitants of these worlds.

It is worth highlighting certain considerations affecting implementation of dark-side illumination. For example, heating the dark side would lower the day–night temperature differential and slow day-to-night heat transfer, warming the day side. The mirrors would also obscure some starlight for day-side inhabitants. Optimally the mirrors could be turned edge-on to our transit line of sight quickly as they exit the zone of usefulness, in order to minimize obscuration, unnecessary exposure to solar radiation, and forces that would alter the orbit. However, some obscuration may be desirable to reduce the stellar flux to the day side and keep planetary temperatures from rising excessively. Obscuration of the day side is not overly large even if the mirrors are not directed edge on, lying between $\sim R_p^3/R_m^3$ and $\sim R_p^2/R_m^2$ depending on the orbital arrangement, where R_m is the orbital radius of the mirror fleet. Satellites in a $3\,R_p$ orbit would decrease the flux by approximately 4%–11%, while a 10 R_p orbit reduces flux by 0.1%–1%.

As a result of these and other considerations, the detailed distribution and orientation of mirrors within the orbiting fleet are likely quite complicated. The orbital distribution and variable incidence angle of the mirrors would affect the actual mirror surface area required, as well as the observed transmittance of the mirror fleet. However, for most of this paper we restrict ourselves to the simplest case and consider the observable impact of a constant-transmittance fleet of mirrors surrounding an extrasolar planet. Near the end of Section 4, we briefly consider alternative transmittance models, while deferring more detailed modeling of mirror fleet transmittance to another time.

3. MODELING EFFECTS OF A CLOUD OF MIRRORS

An orbiting mirror fleet partially blocks starlight just before, during, and after planetary transit. We initially assume the fleet appears in cross-section as a constant-transparency ring around the planet. Although unlikely to be completely accurate, these models highlight the first-order effects of orbiting mirrors on transit light curves. We also neglect the increased light reflected from the now-illuminated planetary dark side, an assumption validated in Section 5.3.

We modeled fleets of orbiting mirrors in two ways. For our standard runs, we adapted the EXOFAST_OCCULTQUAD routines (Eastman et al. 2013) based on the algorithms of Mandel & Agol (2002). This package calculates light curves as a function of the normalized separation of the star and planet centers ($z = d/R_{\rm star}$), which for circular orbits is related to time ($t = 0$ at transit center) by

$$z = \frac{a_P}{R_{\rm star}}\sqrt{(\sin\omega t)^2 + (\cos i\,\cos\omega t)^2}$$

where i is the orbit inclination and a_P and ω describe the radius and angular frequency of the planetary orbit.

The EXOFAST routine is used to produce a light curve for a transit by a planet without mirrors (LC_P), and again to produce

[5] In 2015, launch costs to geosynchronous transfer orbit on Falcon Heavy in 2015 were estimated at $14100 kg^{-1}: http://www.spacex.com/about/capabilities, retrieved on 2015 May 16.

Table 1
Stellar Parameters

Sp Type	$T_{\rm eff}(K)$	$M/M_{\rm Sun}$	$R/R_{\rm Sun}$	$L/L_{\rm Sun}$	$\log(g)$
M8	2660	0.10	0.13	0.0008	4.96
M5	3120	0.21	0.32	0.0079	4.87
M0	3920	0.47	0.63	0.063	4.72
K5	4410	0.69	0.74	0.16	4.62
K0	5240	0.78	0.85	0.40	4.46
G5	5610	0.93	0.93	0.79	4.39
G2	5780	1.00	1.00	1.00	4.35
G0	5920	1.10	1.05	1.26	4.33

a light curve for a transiting object the size of the mirror fleet (LC_O). The fraction of starlight blocked in each case is $B_P = 1 - LC_P$ and $B_O = 1 - LC_O$, respectively. The light blocked by the transparent mirror ring (absorptance $= \alpha = 1$ —transmittance) is therefore $B_M = \alpha(B_O - B_P)$ and the light curve for a planet encircled by the mirror fleet is

$$LC_{\rm tot} = 1 - B_M - B_P = LC_P(1 - \alpha) + \alpha LC_O. \quad (1)$$

The absorptance α and optical depth τ are nearly equivalent for $\alpha \lesssim 0.1$; however, this is not necessarily valid for our simulations.

We assume the effective cross-sectional area of the constant-transparency mirror ring (αA_m) equals the cross-sectional area of the planet (A_P), resulting in an absorptance

$$\alpha = \frac{A_P}{A_m} = \frac{\pi R_P^2}{\pi\left(R_m^2 - R_P^2\right)} = \frac{1}{\left(\frac{R_m}{R_P}\right)^2 - 1}. \quad (2)$$

This is reasonable because any mirrors between Earth and the planet are not illuminated, and thus do not contribute to the area needed to illuminate the dark side at day-side levels. We also assume that mirrors are turned edge-on quickly as they exit the zone of usefulness, i.e., any mirrors in a position that renders them incapable of illuminating the planet's dark side are edge-on, and thus do not contribute to the fleet's absorptance.

Although our standard simulations assume that the mirror fleet provides constant absorptance, we wished to explore the importance of this simplification. We therefore created software to generate a two-dimensional array representing the absorptance of the planet and mirror fleet, and another representing the star. For all runs, the planet radius was set to 100 pixels. We then shifted the relative positions of the two arrays, calculated the transmitted light for each location, and interpolated the resulting light curve onto the same temporal grid used with EXOFAST. This brute-force modeling approach is significantly slower than that already described, but in all constant-absorptance test cases the light curves generated by the two methods differed by at most 0.05% of the transit depth, within the range expected due to pixelization errors. We used this approach to simulate transits for configurations with non-constant absorptance profiles (see Section 4.3).

3.1. Parameterization

Table 1 summarizes the properties of stars used in our transit models. Columns 1–5 contain the spectral type and basic stellar properties from Zombeck (1990). Values for surface gravity $\log(g)$ were estimated in two ways. For Method A, we retrieved information on *Kepler* stars hosting exoplanets from the Exoplanet Data Explorer (Wright et al. 2011) at http://exoplanets.org/table, fit the data with $\log(g) = c_1 + c_2 T_{\rm eff}$, then utilized this function to estimate $\log(g)$. For Method B, we scaled the surface gravity from the solar value, assuming g $\propto M/R^2$. In several test runs, the differences in the resulting light curves were at most 1% of the transit depth, and generally less than 0.2%. For all of our standard runs, we used the values from Method A, as shown in column 6.

For our standard runs, we assumed heavy-element abundances half that of the Sun ($\log([{\rm Fe/H}]_{\rm ratio}) = -0.3$), and calculated quadratic limb-darkening parameters γ_1 and γ_2 using the interface of Eastman et al. (2013; http://astroutils.astronomy.ohio-state.edu/exofast/limbdark.shtml), which interpolates over the values of Claret & Bloemen (2011). The relatively low element abundance value was chosen because we anticipate advanced civilizations around older stars, which tend to be metal-poor.

We assumed circular planetary orbits in all our models. Edge-on orbits were standard, but we also explored other orbit inclinations. To determine appropriate orbit sizes, we estimated each star's HZ using the *optimistic* values of Kopparapu et al. (2013), accessed via http://depts.washington.edu/naivpl/content/hz-calculator. We note that substantial disagreement exists on the precise range of orbits that lie in a star's HZ. For a detailed discussion, see Petigura et al. (2013), who compare the conservative (rather than optimistic) choices made by Kopparapu et al. (2013) with those of other authors (Kasting et al. 1993; Pierrehumbert & Gaidos 2011; Zsom et al. 2013). However, in this paper, we are concerned mainly with illustrating the potential impacts of a fleet of orbiting mirrors on transit light curves, using one plausible choice for the HZ.

Table 2 summarizes the properties of planets used in our transit models. For each stellar spectral type (column 1), the inner edge ($\rm HZ_{in}$) and center ($\rm HZ_{mid}$) of the chosen HZ are indicated in columns 2 and 5. Corresponding planetary orbit periods for circular orbits ($P_{\rm orb,in}$ and $P_{\rm orb,mid}$), determined from stellar mass and orbit size, are in columns 3 and 6. Because we anticipate that mirror fleets might be implemented around planets in synchronous rotation, columns 4 and 7 contain estimates of the tidal synchronization timescale ($\tau_{\rm syn}$) for Earth-like ($M = M_E$, $R = R_E$) planets in these orbits. Planets that would not synchronize within ~10 Gyr are marked with an asterisk (*).

To estimate $\tau_{\rm syn}$, we used Equation (3) of Forget & Leconte (2014), based on the equilibrium theory of tides (Darwin 1880; Hut 1981; Leconte et al. 2010). We followed their lead in estimating tidal dissipation values according to Lunar Laser Ranging experiments of Neron de Surgy & Laskar (1997), which yield

$$\tau_{\rm syn}({\rm Gyr}) = 21.71\frac{\left(M_p/M_E\right)a({\rm AU})^6}{G\left(M_s/M_{\rm Sun}\right)^2\left(R_p/R_E\right)^3}. \quad (3)$$

Terrestrial planets at the *inner edge* of the chosen HZ ($\rm HZ_{in}$) synchronize their rotation within 6 Gyr for all G, K, and M main sequence stars. However, $\tau_{\rm syn}$ is longer for terrestrial planets elsewhere in the HZ. For example, for planets at its *center* ($\rm HZ_{mid}$), synchronous rotation is achieved within ~1 Gyr for main sequence stars K5 and later, but not within 10 Gyr for stars K0 and earlier. Tidal synchronization

Table 2
Planet Parameters

Sp Type	HZ_{in} (AU)	$P_{orb,in}$ (d)	$\tau_{syn,in}$ (Gyr)	HZ_{mid} (AU)	$P_{orb,mid}$ (d)	$\tau_{syn,mid}$ (Gyr)
M8	0.023	3.27	3×10^{-7}	0.043	9.24	1×10^{-5}
M5	0.073	14.8	7×10^{-5}	0.13	37.4	2×10^{-3}
M0	0.20	47.7	6×10^{-3}	0.36	115	0.2
K5	0.32	79.6	5×10^{-2}	0.55	179	1
K0	0.48	138	0.4	0.83	313	11*
G5	0.67	208	2	1.13	455	50*
G2	0.75	237	4	1.26	517	90*
G0	0.84	268	6	1.40	577	100*

Note.
* Earth-like planets in these orbits do not synchronize their rotation within 10 Gyr.

timescales are uncertain at best. Estimates made by Kasting et al. (1993) suggest that for planets orbiting at HZ_{mid}, only those around M stars would be in synchronous rotation at the current epoch, while those orbiting at HZ_{in} around most K stars could also be in this state. Although detailed estimates vary, planets in an M star's HZ are extremely likely to be in synchronous rotation after a several gigayear biological evolution timescale. However, note that a planet's climate and habitability may also be altered by effects such as tidal heating or orbital migration (see Barnes et al. 2008, 2013). Because they are most likely to be in synchronous rotation, we focus on planets around M stars for the majority of our models, but do explore other options, since Earth-like planets orbiting a G star near HZ_{in} might be in synchronous rotation after sufficient time, and as noted earlier, civilizations on Earth analogues might choose to utilize a fleet of mirrors for reasons other than dark-side illumination of a synchronously rotating planet.

In each orbit, we simulated transits for planetary radii of $R_P/R_{\rm Earth} = [0.5, 1, 2]$, corresponding to $M/M_E = [0.125, 1, 8]$ if all have the same average density as Earth, or $M/M_E = [0.53, 1, 5.1]$ using the relationships of Weiss & Marcy (2014). Effects on the transit due to brightness of the planet's dark side were ignored. For each planet, we simulated mirror fleets extending to three different distances from the planet center: $R_m/R_P = [2, 3, 10]$. Mirror fleets that are substantially smaller ($R_m/R_P = \sqrt{2}$) will be nearly opaque according to Equation (2), while those that are substantially larger may have less stable orbits and may suffer from inefficiencies in redirecting starlight.

For all runs, in addition to determining the light curve for the planet surrounded by its mirror fleet ($P + M$), we also determined the light curve for the planet alone (P) and for a larger planet (LP) sans mirrors that produces the same eclipse depth as $P + M$.

4. RESULTS OF SIMULATIONS

Overall, mirror-induced perturbations to the transit shape are similar for all situations. We begin by presenting one model as a reference, then explore the effects of varying stellar, planetary, and mirror fleet parameters. We chose a large terrestrial planet orbiting an M5 star as our reference, because these stars and planetary sizes are relatively common, and a relatively large planet will create a deeper transit with a longer entrance time, making it easier to analyze the transition region potentially affected by the mirror fleet.

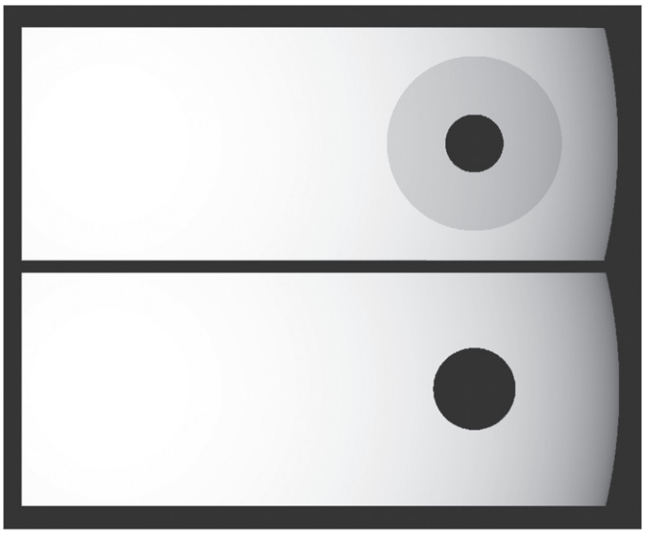

Figure 2. Top panel: simulated image of a planet with $R_P = 2R_{\rm Earth}$, surrounded by a constant-absorptance mirror fleet with $R_m = 3R_P$, transiting in front of an M5 star. Only a strip of the right half of the star is shown. Bottom panel: same as above, but for an isolated planet large enough to produce a transit of the same depth.

The top image in Figure 2 displays our reference simulation: a planet with a radius $R_P = 2R_{\rm Earth}$, surrounded by a constant-absorptance fleet of mirrors with $R_m = 3R_P$, transiting in front of an M5 star. The solid line in the left panel of Figure 3 displays the simulated light curve for the planet and its fleet of mirrors ($P + M$), with the dashed line representing the planet-only transit curve (P). A transit of the same depth as $P + M$ but caused by an isolated LP, as in the bottom of Figure 2) is shown by the dotted line.

Containing many individual reflectors, the translucent mirror fleet blocks some starlight (see Figure 2) and deepens the transit. This $P + M$ case can be distinguished from that of an isolated LP in the timing and shape of the transit ingress and egress light curve. In the initial phases of the transit, only the mirrors block starlight, so the decrease occurs relatively gradually. When the planet itself enters transit, the light curve decreases more rapidly. Later in the sequence, the dimming slows with the planet fully in front of the star while the semi-transparent halo of mirrors continues to occlude more starlight. These effects are seen in the left-hand panel of Figure 3, although the signature is complicated by the presence of stellar

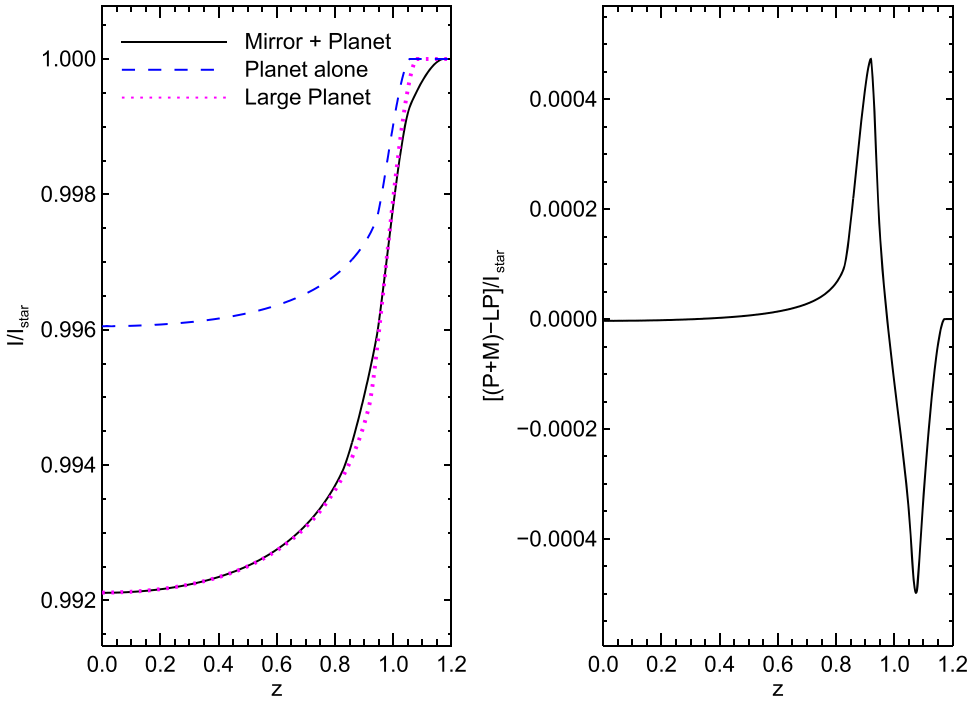

Figure 3. Left panel: transit light curves for a planet with $R_P = 2R_{\rm Earth}$ orbiting an M5 star (dashed line: P), the same planet surrounded by a constant-absorptance mirror fleet extending to 3 planetary radii (solid line: $P + M$), and a planet without mirrors large enough to produce a light curve with the same depth of transit (dotted line: LP). Right panel: difference between the mirror fleet transit light curve ($P + M$) and the one for the solitary large planet (LP), relative to the stellar intensity.

limb-darkening. Note that once the mirrors are fully in front of the star, as depicted in Figure 2, the transit light curve becomes very similar to that of a larger isolated planet, with the small differences caused by variations in stellar brightness across the differing areas of occlusion. The right panel shows the difference of the light curves for the planet plus mirrors transit and the LP transit, highlighting the effects as the planet enters and exits its transit.

Although a fleet of mirrors orbiting an exoplanet affects both the time-span and depth of a transit, it would not affect the timing or depth of the planetary eclipse optical light curve. Once again, a difference in transit and eclipse time span could suggest the presence of mirrors to illuminate a planetary dark side, but the same caveat regarding elliptical planetary orbits applies here as for the single large mirror. We assume that the mirror fleet is designed for maximum efficiency, so all starlight is directed onto the planet and none is re-directed toward us during the eclipse. However, if the fleet does not include efficiency as a primary design constraint, we might observe a temporary *increase* in brightness just before or after the eclipse phase due to spillover effects.

We anticipate no detectable effects due to thermal emission from either a single large mirror or an armada of orbiting mirrors. We assume the back sides are cold, as mirror reflection efficiency is high and no bright IR sources illuminate them from behind. Since light mirrors are very thin, the front and back are at nearly the same cold temperature.

4.1. Effects of Varying Stellar Abundance or Spectral Type

Since the mirror fleet mainly affects transit entry and exit, we questioned whether differences in limb-darkening could exhibit the same signature. One source of uncertainty in limb-darkening arises from abundance variations. In runs for identical planets ($R_P = 2R_{\rm Earth}$, $R_m = 3R_P$), varying the stellar abundance from half-solar to tenth-solar or to full-solar impacted the light curve depth by 0.5%–4%, depending on stellar type. This is of similar magnitude as the effects of a mirror fleet. We therefore created light curves for isolated planets transiting M5 stars with tenth-solar and full-solar abundances, with sizes generating transit depths equal to that for the reference simulation. The solid line in Figure 4 shows the difference of the mirror plus planet and large planet light curves from Figure 3, while the dotted and dashed lines show the difference of the light curves for the isolated planets for

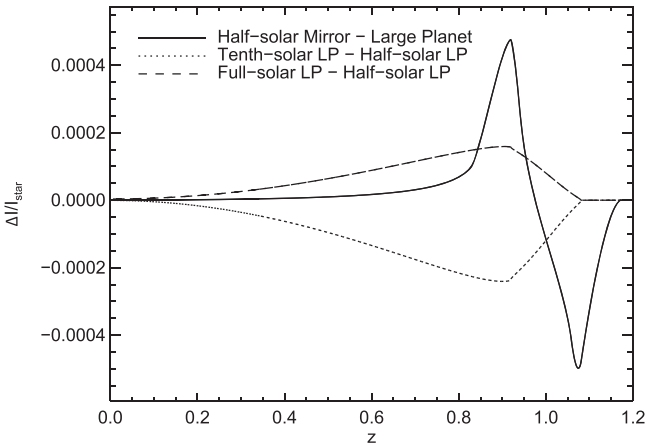

Figure 4. Impact on light curve of abundance-induced limb-darkening variations compared with that of a mirror fleet. The solid line displays the difference (relative to stellar intensity) between light curves produced by a planet surrounded by a mirror fleet and an isolated large planet, both transiting an identical M5 star with half-solar abundance. The other two lines display the difference between the isolated large planet light curve for half-solar abundance and the light curves for isolated planets producing transits of the same depth for tenth-solar abundance (dotted) and full-solar abundance (dashed).

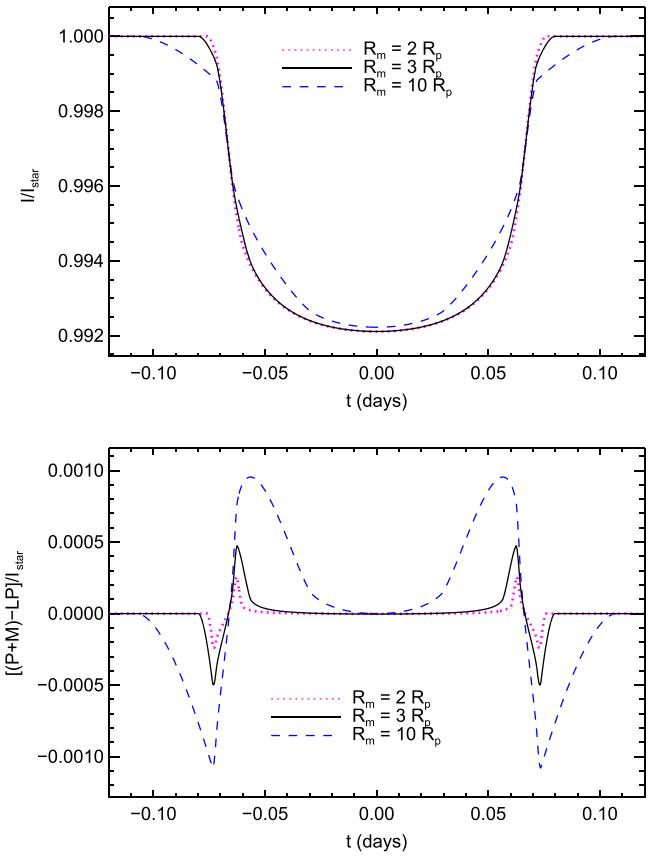

Figure 5. Top panel: transit light curves that result when a planet with $R_p = 2R_{\rm Earth}$, located in the middle of the star's HZ, passes in front of an M5 star. In all cases the planet is surrounded by a constant-absorptance mirror fleet, with $R_m = 3R_P$ (solid), $R_m = 2R_p$ (dotted), or $R_m = 10R_p$ (dashed). Bottom panel: difference between the mirror fleet transit light curve ($P + M$) and the one for a solitary larger planet (LP) that would produce the same depth of transit, relative to the stellar intensity, for the same situations.

various stellar abundances. Different stellar abundances cannot be mistaken for the effects of a transiting planet surrounded by a fleet of mirrors because limb-darkening variations have a fundamentally different signature.

Although not displayed, we simulated transits of planets orbiting the full range of stellar types displayed in Table 1. Transit light curve details differ somewhat for stars of earlier spectral types. In particular, (1) differences in limb-darkening affect the detailed shape of the light curve near entry and exit. (2) For larger stars, the same planet plus mirror fleet blocks a smaller fraction of light, resulting in a shallower transit, and the mirror fleet's effects last a smaller fraction of the transit time span. Compared with an isolated planet transit of the same depth, the impact of the mirrors is of the order of $10^{-4}I_{\rm star}$ for an M0 star, roughly a factor of 2 smaller for a G2 star, and several times larger for an M5 star. (3) Longer orbital periods, corresponding to the larger HZ orbits around earlier-type stars, increase the time span of transits for these planets. Despite these differences, simulating transits of other stars does not significantly change the bipolar signature of the mirror fleet in transit residuals. In addition, the maximum residuals remain approximately the same relative to transit depth for all stellar types (e.g., ∼4%–6% for $R_P = 2R_{\rm Earth}$, $R_m = 3R_P$).

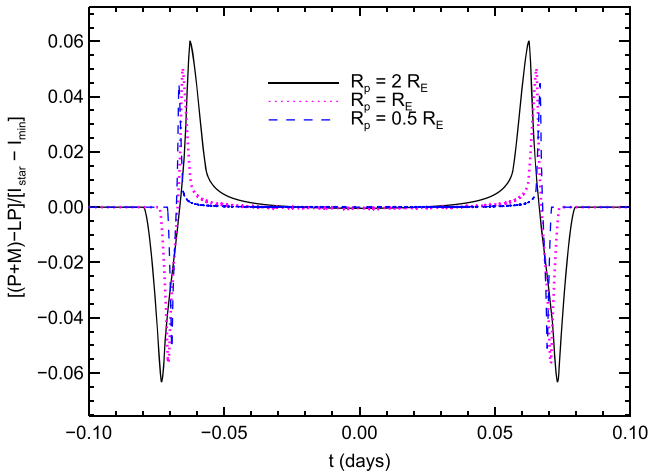

Figure 6. Impact of a fleet of mirrors with $R_m = 3R_P$ on transits for planets of various sizes orbiting in the middle of an M5 star's HZ. The lines show the difference between the light curve resulting from the planet plus mirror (P + M) transit and one of the same depth resulting from an isolated larger planet (LP) transit for planets with $R_P/R_{\rm Earth} = 0.5$ (dashed), 1.0 (dotted), and 2.0 (solid).

4.2. Varying Mirror Fleet Extent, Planetary Size, or Orbit Inclination

The top panel of Figure 5 displays light curves for transits that are identical to the reference simulation apart from the mirror fleet's extent. Larger fleets affect the light curve for a larger fraction of the transit duration, with more dramatic departures from the isolated planet situation. The dashed curve ($R_m = 10R_P$) has a slightly different transit depth because $R_P/R_{\rm star} = 0.057 so R_m/R_{\rm star} = 0.57$; the mirror fleet extends across a significant fraction of the stellar surface, which has different intensities at different locations due to limb-darkening. Because all mirror fleets have the same effective area, the larger fleet has a lower absorptance. So at $z = 0$ the smaller, more opaque systems block light primarily from the star's brighter central regions, while the largest, most transparent one transmits more of that light, instead blocking less intense outer portions of the star. The bottom panel illustrates that, all else being equal, mirror fleets with large spatial extents would be more apparent in transit light curve abnormalities than those with smaller spatial extent, both temporally and in the magnitude of the effect on transit residuals.

For mirror fleets such as those in the reference model, we explored the effects of varying planet size. Figure 6 displays the difference between the $P + M$ and LP light curves, relative to transit depth $I_{\rm star} - I_{\rm min}$, for three sizes of terrestrial planets, each orbiting at $\rm HZ_{mid}$ around an M5 star. Smaller planets result in transits of substantially shallower depth; however, in all cases, the mirror fleet has a significant impact (a few percent of the transit depth) on the entrance and exit light curves. The duration of the largest residuals is shorter for smaller planets.

All previous results are for edge-on orbits, so the minimum projected distance between star and planet centers is $z_{\rm min} = 0$. The top panel of Figure 7 compares this situation (solid line) with orbits that are not exactly edge-on ($z_{\rm min} \neq 0$). For these, a planet with $R_P = 2R_E$ and $R_m = 10R_P$ is located at $\rm HZ_{mid}$ around an M5 star. The dashed line planet transits at $z_{\rm min} = 0.75$, so part of the mirror fleet never occludes the star ($R_m/R_{\rm star} = 0.57$). In the dotted line case, the planet center crosses the edge of the star ($z_{\rm min} = 1$), and for the dash–dotted

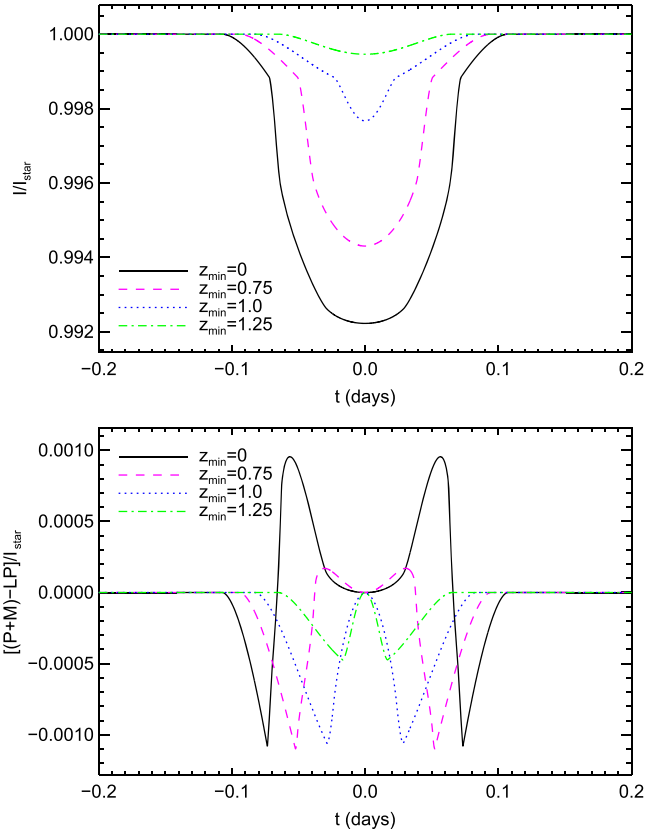

Figure 7. Top panel: transit light curves that result when a planet with $R_p = 2R_{\rm Earth}$, located in the middle of the star's HZ, passes in front of an M5 star. In all cases, the planet is surrounded by a constant-absorptance mirror fleet with $R_m = 10R_P$. The four curves result from different values for the impact parameter: $z_{\rm min} = 0$ (solid), $z_{\rm min} = 0.75$ (dashed), $z_{\rm min} = 1$ (dotted), and $z_{\rm min} = 1.25$ (dash–dotted). Bottom panel: difference between the mirror fleet transit light curve ($P + M$) and the one for a solitary larger planet (LP) that would produce the same depth of transit, relative to the stellar intensity, for the same situations.

light curve ($z_{\rm min} = 1.25$) the planet itself never crosses in front of the star, but the mirrors still create a transit. For each impact parameter $z_{\rm min}$, the bottom panel of Figure 7 shows the difference of the $P + M$ and LP light curves. This figure reveals that as $z_{\rm min}$ increases, the mirror effects are evident during a greater fraction of the transit timescale. As long as more than half of the planet crosses in front of the star, i.e., $z_{\rm min} < 1$, the transit residuals display a bipolar signature of the mirror fleet's presence. For $z_{\rm min} > 1$, the residuals are no longer bipolar, but the mirror fleet produces transits that last much longer than would be appropriate for the transit depth in the absence of mirrors, and the light curve minimum is not at transit center.

4.3. Effects of Different Mirror Density Distributions

Having explored the first-order effects of a fleet of mirrors, we considered alternative transmittance models based on actual distributions of steerable mirrors, which required our brute-force approach. The simplest such situation is with mirrors evenly distributed (density $\rho_{\rm mirr}$) within a spherical shell ($R_i \leqslant r \leqslant R_o$) around the planet. Although not necessarily realistic, this scenario lets us explore the importance of our constant-absorptance assumption. We calculated the absorptance at each projected radial distance based on the projected

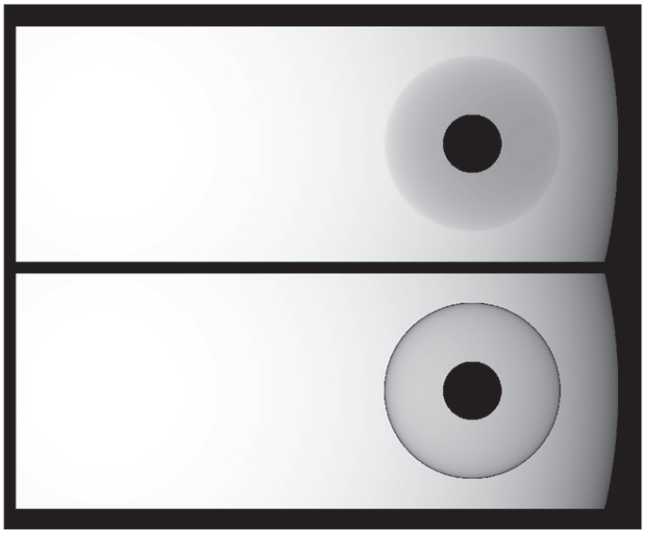

Figure 8. Top panel: simulated image for the same situation as Figure 2 but for a planet surrounded by a constant-density fleet of mirrors in a thick shell extending from just above the planet's surface (from 1.01 R_P to $3R_P$). Bottom panel: same as above, but the mirrors are distributed in a thin shell extending from 2.99 R_P to $3R_P$.

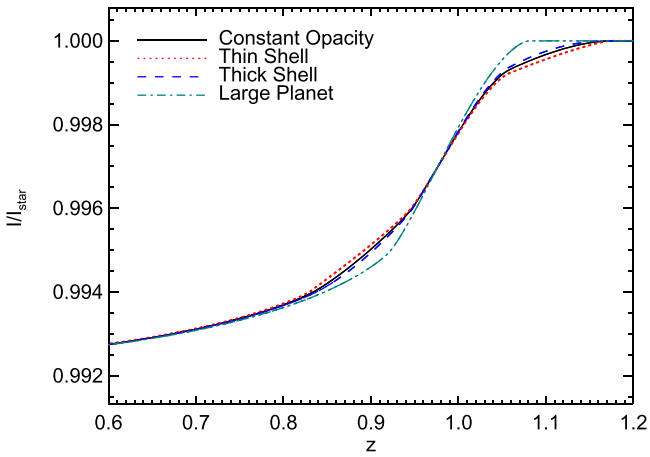

Figure 9. Transit light curves for different absorptances. The solid line displays the light curve of a transit produced by a planet with $R_p = 2R_{\rm Earth}$, and a constant-absorptance fleet of mirrors extending outward to $R_m = 3R_p$, crossing in front of the center of an M5 star with half-solar abundance. The dotted and dashed lines display the transit light curve produced by thick ($R_i = 1.01R_p$) and thin ($R_i = 2.99R_p$) constant-density shells of mirrors, respectively, each with an outer radius of 3 R_p. The dash–dotted line is the light curve for an isolated planet large enough to produce a transit of the same depth.

density of the fleet:

$$\rho_{\rm proj} = 2\rho_{\rm mirr}\left(\sqrt{R_o^2 - r^2} - \sqrt{R_i^2 - r^2}\right) \quad (r < R_i)$$
$$\rho_{\rm proj} = 2\rho_{\rm mirr}\left(\sqrt{R_o^2 - r^2}\right) \quad (R_i \leqslant r \leqslant R_o). \qquad (4)$$

The absorptance was again normalized so the total light intercepted equals that normally incident on the planet, while simultaneously ensuring absorptance $\alpha \leqslant 1$. We considered two extremes: a thick uniform shell of mirrors extending outward from just above the planet's surface, and mirrors all at nearly the same altitude. In the former case, the mirror fleet's collective absorptance is largest near the planet's surface (near

R_i), gradually decreasing to zero at the fleet's outer extent. For the thin-shell case, the absorptance is small near the planet's surface, increasing with distance, then sharply peaked near the fleet's altitude. Figure 8 illustrates the extreme differences in absorptance profiles for the thick-shell (top panel) and thin-shell (bottom panel) cases.

These simulations illustrate the relative insensitivity of transit light curves to varying mirror-fleet absorptance profiles. Figure 9 compares transit light curves for these two cases with previously discussed results. The constant-absorptance and large planet light curves are the same as those shown in Figure 3. The dotted line results from a thin shell of mirrors ($R_i = 2.99R_p$, $R_m = 3R_p$), and the dashed line from a thick shell of mirrors extending from $R_i = 1.01R_p$ to $R_m = 3R_p$. The inner radii in both extremes were chosen based on the resolution of our brute-force simulations (planet radius = 100 pixels). From this figure, it is apparent that light curves for various absorptance distributions are more similar to each other than they are to that for an isolated planet. Our simple constant-absorptance model therefore captures the dominant effects of this method of dark-side illumination.

5. PROSPECTS FOR DETECTION

We now consider the potential detectability of such mirror installations, focusing on the predicted ($P + M$) light curve for an Earth-sized planet ($R_P = R_{\rm Earth}$) orbiting a G2 star at $HZ_{\rm in}$, surrounded by a large ($R_m = 10R_P$) constant-absorptance fleet of mirrors. We chose this situation in part because the only known civilization evolved on such a planet. Older M stars are very common, and their potentially habitable terrestrial planets are likely in synchronous rotation. However, they are fainter, and thus not necessarily better candidates when seeking signatures of planetary-scale engineering. Recall that a planet near $HZ_{\rm in}$ for a G2 star might be synchronously rotating at this time (see Section 3.1), or that civilizations might choose to affect the climate of bodies other than their planet of origin.

5.1. Detectability with Kepler

Until now we have neglected the reality that a mirror fleet's effects will be partially suppressed by transit fitting routines through variations in orbit inclination or stellar limb-darkening. To assess this, we re-sampled our $P + M$ model onto *Kepler*'s short cadence (SC) timescale for three transits. We used the Transit Analysis Package (TAP, Gazak et al. 2012) to fit an isolated planet model to the simulated light curve, restricting limb-darkening parameters to a range appropriate for stars with effective temperatures within 750 K of a G2 star. Because the fleet is translucent ($\alpha \sim 0.01$ for $R_m = 10R_P$), predicted residuals ($\sim 10^{-5} I_{\rm star}$) are substantially smaller than those for the Jupiter-scale opaque structures of Arnold (2005), and thus too small to detect in *Kepler* data.

To confirm this, we simulated "best-case scenario" *Kepler* data for our $P + M$ model and compared the residuals for the previously determined isolated planet model with the difference between the $P + M$ model and the isolated-planet TAP model determined above (hereafter TAP IPM). Given the relatively long orbital period (~237 days) for a planet orbiting a G2 star at $HZ_{\rm in}$ ($a = 0.75$ AU), at most six transits of data are available. Kepler 10 is a relatively bright ($Kp = 10.96$) G2 star in the *Kepler* sample, with instrumental and photon noise estimated by the *Kepler* pipeline as ~200 parts-per-million (ppm) for SC data. We simulated six transits of SC data with Gaussian white noise at this noise level, although we note that Batalha et al. (2011) report more long-cadence noise (~62 ppm) than the *Kepler* pipeline estimate (~36 ppm).

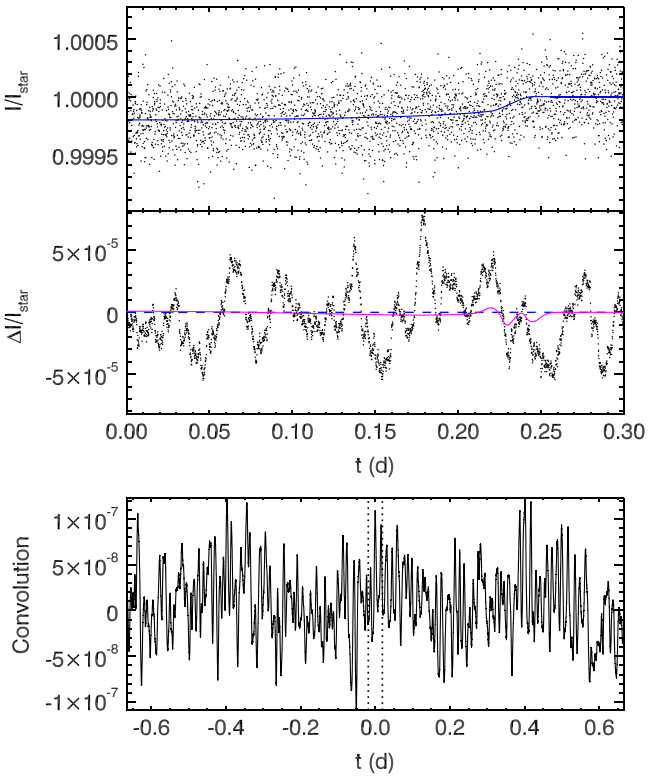

Figure 10. Top panel: simulated phase-folded data with 200 ppm noise and *Kepler* SC sampling for six transits of a planet with $R_P = R_{\rm Earth}$ and $R_m = 10R_P$, orbiting around a G2 star at 0.75 AU. Only half of the transit is displayed. The solid line is the best-fit isolated planet model produced by TAP analysis of the noiseless $P + M$ model. Middle panel: smoothed simulated residuals (dots) of the simulated data and TAP model shown in the top panel, and predicted residuals (solid line) based on the difference between the isolated planet TAP model and the simulated $P + M$ model. The smoothing length for both was determined by half of the timescale $t_{1/2}$ (defined in the text). Bottom panel: convolution of the unsmoothed simulated and predicted residuals. The vertical dotted lines indicate $\pm t_{1/2}$, and relate to the statistical analysis described in the text regarding Figure 11.

The top panel of Figure 10 displays the phase-folded simulated data, where we retain the folded timescale for convenience in later analysis and $t = 0$ represents the center of each transit. For clarity, only half of the transit is displayed. The superimposed solid line is the TAP IPM described above, i.e., the one that best fits the noiseless $P + M$ model used to simulated the data. The residuals between our noisy data and the TAP IPM, smoothed for visual clarity, are shown in the middle panel. They are overlaid (solid line) by the smoothed difference between our $P + M$ model and the TAP IPM. Clearly, noise in these data overwhelms any potential mirror fleet signal. In the bottom panel, the convolution of the (unsmoothed) simulated and predicted residuals confirms that they are uncorrelated.

M stars are substantially dimmer at visible wavelengths, resulting in noisier data. A typical *Kepler* catalog star has a magnitude of ~14, based on information retrieved from the Exoplanet Data Explorer (Wright et al. 2011), but the median M star is fainter than $Kp = 15$. Kepler 138, hosting multiple terrestrial planets (Kipping et al. 2014; Rowe et al. 2014), is an

unusually bright Kepler M0-dwarf at $Kp = 12.93$, but still two magnitudes fainter than the G2 star simulated below. Thus the expected noise level would be ~2.5 times greater. Because of the shorter orbital period for a planet at HZ_{in} around an M0 star, up to five times more transits of *Kepler* data could be available, mitigating the additional noise. However, mirror fleets around these stars would still be undetectable in *Kepler* data.

5.2. Future Prospects for Detection

The *James Webb Space Telescope* (*JWST*) will have a collecting area of 25 m^2, 35 times larger than *Kepler* (0.708 m^2). Using area, quantum efficiency, and filter transmission parameters provided in Van Cleve & Caldwell (2009) and http://ircamera.as.arizona.edu/nircam/features.html, along with the Planck blackbody function for a G2 star, we computed the expected count rate of the NIRCAM F150W2 filter relative to the *Kepler* full bandpass. The *JWST* F150W2 count rate will be ~45 times that for *Kepler*, reducing noise levels to $\sim 200/6.7 = 30$ ppm.

M stars emit a larger fraction of their light at IR wavelengths, so we used the effective temperatures and radii of Table 1 to calculate the relative expected *JWST* photon rates for G2, M0, and M5 stars at equal distances. In the F150W2 bandpass, we expect 6.7 and 53 times more photons from a G2 star than for M0 and M5 stars, respectively. Data for M stars at similar distances will be noisier, requiring more transits to achieve detections, so only the closest and brightest M stars will be feasible targets for *JWST*.

As before, we simulated data with SC sampling for an Earth-like planet orbiting at a G2 star's HZ_{in} using our $P + M$ model, but at *JWST*'s expected noise level of 30 ppm. We compared the residuals between the simulated data and the TAP IPM with the difference between the $P + M$ model (used to simulate the data) and the TAP IPM. We did this comparison for 100 separate realizations of noise for each of 2, 3, 4, 5, and 10 transits of *JWST* data. Although we would ideally base our comparisons on isolated-planet TAP models fit to each simulated noise realization, this simplified first-order analysis is sufficient to illustrate the key points regarding mirror fleet detectability.

The top panel of Figure 11 shows the phase-folded data for a four-transit noise realization, along with the TAP IPM. For visual clarity, only half of the transit is displayed; however, all analyses were performed using the full-transit simulated data. The smoothed residuals in the middle panel reveal the signature of the mirror fleet; residuals of the simulated data and TAP IPM (dots) are compared with predicted residuals (solid line; difference between simulated noiseless $P + M$ model and TAP IPM). Both are smoothed by half of the timescale $t_{1/2}$ (defined below) for visual clarity. The convolution in the bottom panel demonstrates the significant correlation between the (unsmoothed) simulated residuals and the predicted model difference. Vertical dotted lines delineate points satisfying $|\Delta t| \leqslant t_{1/2}$, where $t_{1/2}$ is the timescale for the isolated planet model light curve to decrease from maximum to half of the transit depth. The peak is 5.49σ above the convolution function's mean, with both mean and rms (σ) determined by data outside the region delineated by $|t_{1/2}|$, i.e., where we do not expect a significant signal. We display this instance of noise because its convolution peak significance (5.49σ) equals the median significance for the 100 separate four-transit noise realizations.

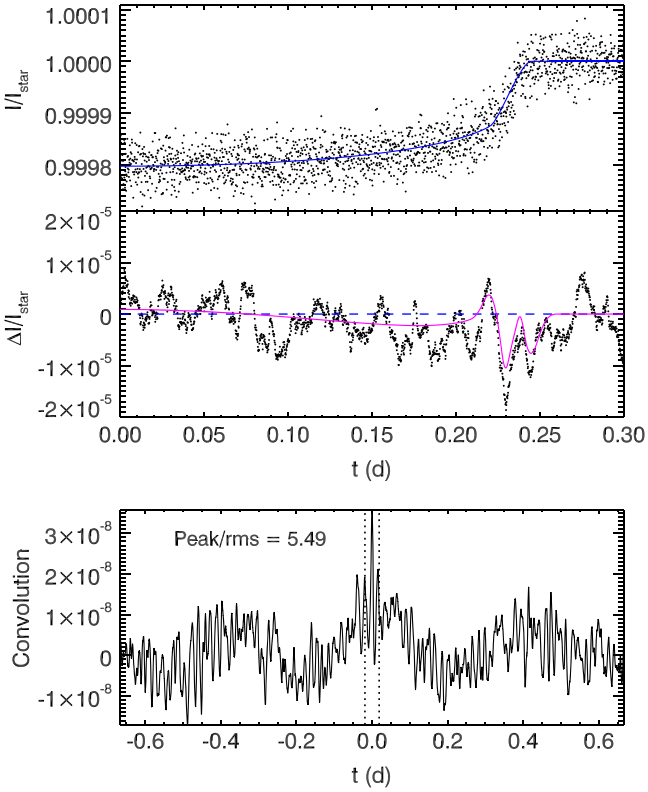

Figure 11. Same as Figure 10 but for four transits of simulated data with a noise level of 30 ppm, as anticipated for *JWST*.

In the 165 points with $|\Delta t| \leqslant t_{1/2}$, the probability of the convolution having a peak of at least this significance occurring by chance is $4.4 \times 10^{-4}\%$. Of the 100 instances of four transits with white Gaussian noise of 30 ppm, the convolution peak was at least 4σ 94 times. In our five-transit simulations, 99/100 have convolution peaks of 4σ or higher, with a median of 6.10σ, and a probability of random occurrence no greater than ~2% in all 100 realizations. Thus for a star like Kepler-10, we anticipate successful detection of such a mirror fleet with data for only a moderate number of transits.

Could the effects of dark-side illumination be detectable with fewer transits? For the 100 separate three-transit realizations, the median significance of the convolution peak was 4.78σ, with 83/100 occurring at 4σ or above. For the two-transit realizations, the median peak significance was 3.90σ, with only 44/100 reaching the 4σ threshold. We conclude that at this 30-ppm noise level, spurious low-significance detections become increasingly likely with fewer than four transits of data.

An initial impression of the four-transit residuals as shown might suggest the isolated planet fit is adequate, therefore, mirror fleet signatures could go unnoticed without a correlation analysis similar to that carried out above. However, for 10-transit simulations, the convolution analysis results in a peak above 4σ 100% of the time, with a probability of the weakest peak occurring by chance of <0.06%. Figure 12 displays the results of a 10-transit simulation with a peak of median significance (7.74σ). In this situation, the simulated smoothed residuals do indicate that the isolated planet model is insufficient, and the high significance of this signature is made

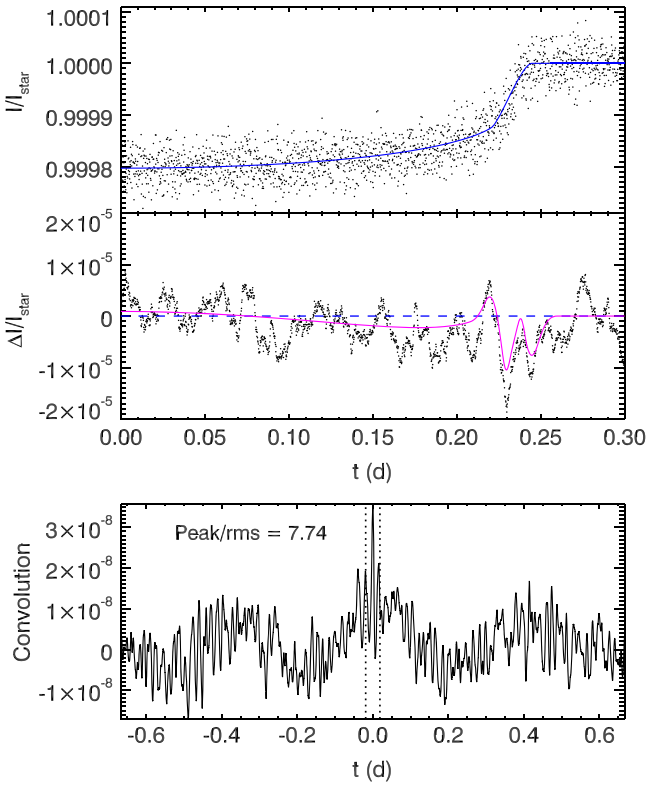

Figure 12. Same as Figure 10, but for 10 transits of simulated data with a noise level of 30 ppm, as anticipated for *JWST*.

apparent by the strong peak in the convolution shown in the bottom panel. The probability of this peak occurring at random is only 2.7×10^{-10}%.

Residuals could be further suppressed if the isolated-planet TAP models do not restrict the range of limb-darkening parameters to values appropriate for similar stars. However, in the majority of cases the stellar temperature and spectral type are known sufficiently well to support the use of some restrictions.

The *Transiting Exoplanet Survey Satellite* (*TESS*), observing at 600–1000 nm, may identify transiting exoplanets for which targeted *JWST* observations would be sufficient for our purpose (Ricker 2014; Ricker et al. 2014). *TESS* will look at stars 30 to 100 times brighter than *Kepler* ($5 \lesssim m \lesssim 12$), across the full sky. Primarily sensitive to orbital periods of up to 60 days, it can detect longer orbital periods in regions of the sky coinciding with *JWST*'s continuous viewing zone (CVZ). It will study primarily F, G, and K stars, but also all of the M dwarfs within 200 light years. It is anticipated that *TESS* will identify ~300 transiting super-Earths and tens of Earth-sized planets, with $\sim 1/3$ of them in or near the CVZ. *TESS* might well discover Earth-sized exoplanets in the HZs of K or M stars bright enough for detailed follow-up observations with *JWST* or future ground-based 30 m class telescopes. Since high-quality transit data on such planets are of great interest for studying properties such as their atmospheres, data adequate for the task of identifying or ruling out fleets of orbiting mirrors will become available.

5.3. Second-order Effects and Potential False Positives

Since orbiting mirrors illuminate the planet's dark side, we explored the importance of planetary reflection of this light. We assume the planetary contribution to photons received is constant, and that the amount of starlight reaching the day side equals that reaching the "dark" side via mirrors. The planet to stellar flux ratio is therefore on the order of

$$\frac{F_P}{F_{\rm star}} = \left(\frac{R_P}{R_{\rm star}}\right)^2 \left(\frac{A}{2\pi}\right)\left(1 - \frac{\alpha}{2}\right).$$

The first factor represents the fraction of total starlight intercepted by the cross-sectional area of the planet. A is the planet's albedo, i.e., the fraction of starlight that is scattered, with division by 2π because it scatters into 2π sr. The final factor accounts for dimming of scattered planetary light by the mirror fleet; absorptance is reduced because only half the mirrors lie on our side of the planet. Greater effects occur for planets that are large relative to the stellar size. For small M8 stars, a planet with $R_P = 2R_{\rm Earth}$ has radius $R_P = 0.14R_{\rm M8}$. For a mirror fleet extending to $R_m = 3R_P$, the absorptance (given our assumptions) is $\alpha = 0.125$. Assuming a planetary albedo comparable to Earth's ($A = 0.3$), this contribution alters the observed transit depth by at most 0.089%, significantly less than the 4%–6% due to mirror fleets (see end of Section 4.1). Thus scattered light from the now-illuminated dark side produces only a small effect on a transit light curve.

Since *JWST* and other future telescopes will observe primarily in the IR, we must consider thermal radiation from the now-warmed dark side. The planet to stellar flux ratio at any particular wavelength is

$$\frac{F_P(\lambda)}{F_{\rm star}(\lambda)} = \frac{\epsilon B_\lambda(T_P)}{B_\lambda(T_{\rm star})}\left(\frac{R_P}{R_{\rm star}}\right)^2$$

where $B_\lambda(T)$ is the Planck thermal blackbody radiation, and ϵ is the planet's emissivity. An upper limit is achieved by assuming $\epsilon = 1$ and choosing the coolest, smallest star (M8). For an M8 star, $R_P/R_{\rm star} = 0.14$ and $T_{\rm star} = 2660$ K; we assume a habitable planet with $T_P = 300$ K. In the *JWST* bandpass (0.6–28.5 μm), the flux ratio reaches a maximum of 0.09% at a wavelength of 28.5 μm. At the wavelength of strongest planetary emission (~10 μm), the flux ratio is only 0.01%. The change in transit depth is significantly smaller than the 4%–6% effects of orbiting mirrors. Even if $T_P = 1000$ K, planetary thermal radiation only alters the transit depth by 0.7%.

In general, any potential detection of intelligence must be confirmed using an entirely different method. We must consider whether natural phenomena could mimic signs of intelligence. In particular, a face-on ring system is extremely similar to the translucent projected annulus of our putative fleet of mirrors. Several groups have modeled transit detectability of ring systems (Barnes & Fortney 2004; Ohta et al. 2009; Tusnski & Valio 2011), generally focusing on gas giant rings. No known terrestrial planet has a ring system, and we question the stability of such a system around a terrestrial planet in tidally induced synchronous rotation, particularly since Ohta et al. (2009) found that rings around all close-in planets are likely to be short-lived and nearly edge-on, rendering them more difficult to detect. More importantly, ring particles are likely warmer than the mirrors, emitting significantly in the IR thus reducing the IR transit depth. Comparison of IR and optical light curves will therefore help discriminate between

natural and engineered systems, given sufficient sensitivity. Ring systems may also be distinguished from mirror fleets by the effects of forward scattering of light by ring particles, causing flux to brighten just before and after planetary transit (Barnes & Fortney 2004).

Planets in an M star's HZ might experience atmospheric erosion, due to strong stellar activity and weak planetary magnetic moments (e.g., Lammer et al. 2007 and discussions in Scalo et al. 2007 and Tarter et al. 2007). The excess absorption around the planet could produce a similar transit light-curve signature; however, mirrors are equally opaque at all visible wavelengths, while atmospheric transmission exhibits wavelength-dependent features. Extensive optical/UV transit spectroscopy observations of atmospheric escape from hot jupiters HD 209458b reveal that escaping material contains elements such as H, C, O, and Na (see for example, Charbonneau et al. 2002; Linsky et al. 2010; Ehrenreich 2011), effects not expected for engineered structures. Lyα transit observations of HD 189733b show temporal variability in the evaporating atmosphere (Lecavelier des Etangs et al. 2012), whereas a stable mirror fleet will produce no such fluctuations. As a related example, Rappaport et al. (2012) explain transit depth variability for KIC 12557548 b with a trailing cloud of material escaping a disintegrating super-Mercury; this phase-folded transit light curve exhibits substantial asymmetries. Here transit depth should depend on wavelength, although multi-wavelength studies have not yet detected this (Croll et al. 2014). In detailed modeling by Brogi et al. (2012), a pre-transit flux excess is due to forward scattering by dust, another feature not anticipated with a mirror fleet designed for optimal efficiency.

Kipping (2014) finds that bipolar residual signatures (somewhat different in functional form from those discussed in Section 4) can result from uncorrected low-amplitude transit timing variations or from uncorrected variations in transit duration. In principle, through trial and error it should be possible to offset variations in either transit timing or transit duration and sharpen the transit entry and exit for the folded light curve, making residuals consistent with those for an isolated planet. However, if the bipolar residuals are due to a mirror fleet, they will not be improved by any small adjustments to the timing or duration of each eclipse. Each subsesquent transit would make the difference more pronounced. Substantial technological improvements should eventually yield sensitivity sufficient for detailed analysis of individual transit light curves, in which case the mirror fleet would be clearly distinguishable from these effects.

6. CONCLUSIONS

An orbiting fleet of mirrors poses significant but possibly not insurmountable environmental, economic, and engineering challenges, and thus could plausibly be utilized to redirect starlight onto a planet, perhaps to illuminate its dark side. Differences in the time span of planetary transits compared with planetary eclipses could be one indication of the presence of such structures, which would also affect the transit light curve.

We modeled transit light curves resulting from such fleets; compared with an isolated-planet transit of the same depth, the transit with orbiting mirrors begins earlier and reaches its minimum more gradually, with differences most apparent near transit entry and exit. The characteristic signature is not plausibly reproduced by alterations in limb-darkening due to abundance variations. Regardless of stellar type, the difference is typically 4%–6% of the transit depth for mirrors extending 3 planetary radii beyond a planet with $R_P = 2R_{\rm Earth}$. Alterations to planetary scattered light and thermal emission caused by the mirrors are negligible compared to the mirrors' effects on the light curve. For smaller stars, mirror fleets alter transit depth by a larger fraction of the total starlight. The difference is on the order of $10^{-4}I_{\rm star}$ for an M0 star, roughly a factor of 2 smaller for a G2 star, and several times larger for an M5 star. Effects on light curves are most apparent for large planets and mirror fleets of large radial extent. For orbital inclinations $|i|$ less than 90°($z_{\rm min} \neq 0$), mirror effects are evident during a greater fraction of the transit timescale, and produce inconsistencies between transit depth and time. Variations in mirror fleet distribution produce very small alterations in the light curve, so a constant-absorptance model sufficiently captures the main features of such an engineering structure.

The mirror installations considered here are undetectable in the existing *Kepler* data. However, with appropriate analysis, they could be revealed in *JWST* observations, were they present. Natural systems, such as rings or an evaporating atmosphere, might produce light curves with a similar signature, but the effects will vary with wavelength quite differently than the mirror fleet case. With sufficient follow-up observations and sensitivity, a mirror fleet should be distinguishable from these effects.

These models likely do not accurately represent a realistic fleet of orbiting mirrors each adjusting its attitude to maintain a desired illumination pattern. We anticipate this effect is of similar scale to differences in mirror fleet geometry. Future work will include detailed modeling of the absorptance/transmittance of plausible mirror fleets, incorporating consideration of the optimal range of mirror orbit size and eccentricity to provide appropriate illumination, and variations of mirror angle throughout the orbit. A similar effort needs to be made on whether stable mirror orbits are achievable considering tidal effects of the star and radiative effects of the illumination on the thin mirrors, as well as the feasibility of propulsion systems capable of sustaining orbits under these conditions.

This research has made use of the Exoplanet Orbit Database and Exoplanet Data Explorer at exoplanets.org and NASA's Astrophysics Data System. During this work E.J.K. was supported in part by NASA grant NNX09AN69G and donations from the Friends of SETI@home (setiathome.berkeley.edu). E.J.K. would like to thank S.M.S. for allowing him the honor of first authorship for conceiving the original idea and describing the basic analysis technique, despite the fact that S.M.S. executed most of the work and did most of the writing.

REFERENCES

Arnold, L. F. A. 2005, ApJ, 627, 534
Barnes, J. W., & Fortney, J. J. 2004, ApJ, 616, 1193
Barnes, R., Mullins, K., Goldblatt, C., et al. 2013, AsBio, 13, 225
Barnes, R., Raymond, S. N., Jackson, B., & Greenberg, R. 2008, AsBio, 8, 557
Batalha, N. M., Borucki, W. J., Bryson, S. T., et al. 2011, ApJ, 729, 27
Bowyer, S., Werthimer, D., Donnelly, C., et al. 1997, in IAU Coll. 161, Astronomical and Biochemical Origins and the Search for Life in the Universe, ed. C. S. Cosmovici, S. Bowyer & D. Werthimer (Cambridge: Cambridge Univ. Press), 667
Brogi, M., Keller, C. U., de Juan Ovelar, M., et al. 2012, A&A, 545, L5

Bryant, R. G., Seaman, S. T., Wilkie, W. K., Miyauchi, M., & Working, D. C. 2014, in 3rd Int. Symp. on Solar Sailing, ed. M. Macdonald (Berlin: Springer), 525
Carrigan, R. A., Jr. 2009, ApJ, 698, 2075
Carrigan, R. A., Jr. 2012, AcAau, 78, 121
Charbonneau, D., Brown, T. M., Noyes, R. W., & Gilliland, R. L. 2002, ApJ, 568, 377
Claret, A., & Bloemen, S. 2011, A&A, 529, A75
Croll, B., Rappaport, S., DeVore, J., et al. 2014, ApJ, 786, 100
Darwin, G. H. 1880, RSPT, 171, 713
Dressing, C. D., & Charbonneau, D. 2013, ApJ, 767, 95
Dyson, F. J. 1960, Sci, 131, 1667
Eastman, J., Gaudi, B. S., & Agol, E. 2013, PASP, 125, 83
Ehrenreich, D. 2011, European Physical Journal Web of Conferences, 11, 03006
Engle, S. G., Guinan, E. F., & Mizusawa, T. 2009, AIP Conf. Ser., 1135, 221
Forget, F., & Leconte, J. 2014, RSPTA, 372, 30084
Freitas, R. A., Jr. 1983, JBIS, 36, 501
Gaidos, E. 2013, ApJ, 770, 90
Gazak, J. Z., Johnson, J. A., Tonry, J., et al. 2012, AdAst, 2012, 697967
Grenfell, J. L., Grießmeier, J.-M., von Paris, P., et al. 2012, AsBio, 12, 1109
Griffith, R. L., Wright, J. T., Maldonado, J., et al. 2015, ApJS, 217, 25
Henry, T. J., Jao, W.-C., Subasavage, J. P., et al. 2006, AJ, 132, 2360
Howard, A., Horowitz, P., Mead, C., et al. 2007, AcAau, 61, 78
Hut, P. 1981, A&A, 99, 126
Jugaku, J., & Nishimura, S. 2004, in IAUS 213, Bioastronomy 2002: Life Among the Stars, ed. R. Norris & F. Stootman (San Francisco, CA: ASP), 437
Kardashev, N. S. 1964, SvA, 8, 217
Kasting, J. F., Whitmire, D. P., & Reynolds, R. T. 1993, Icar, 101, 108
Kipping, . M. 2014, MNRAS, 440, 2164
Kipping, D. M., Nesvorný, D., Buchhave, L. A., et al. 2014, ApJ, 784, 28
Kopparapu, R. K. 2013, ApJL, 767, L8
Kopparapu, R. K., Ramirez, R., Kasting, J. F., et al. 2013, ApJ, 765, 131
Korpela, E. J., Anderson, D. P., Bankay, R., et al. 2011, Proc. SPIE, 8152, 815212
Lammer, H., Lichtenegger, H. I. M., Kulikov, Y. N., et al. 2007, AsBio, 7, 185
Lecavelier des Etangs, A., Bourrier, V., Wheatley, P. J., et al. 2012, A&A, 543, L4
Leconte, J., Chabrier, G., Baraffe, I., & Levrard, B. 2010, A&A, 516, A64
Lima, M. D., Fang, S., Lepró, X., et al. 2011, Sci, 331, 51
Linsky, J. L., Yang, H., France, K., et al. 2010, ApJ, 717, 1291
Mandel, K., & Agol, E. 2002, ApJL, 580, L171
Marcy, G. W., Isaacson, H., Howard, A. W., et al. 2014, ApJS, 210, 20
Marcy, G., Howard, A., & Johnson, J. 2013, Discovery of Earth-like Planets and Signals from Intelligent Life, Templeton Foundation New Frontiers in Astronomy and Cosmology Grant
Mulders, G. D., Ciesla, F., Pascucci, I., & Apai, D. 2014, in The Water Content of Exo-earths in the Habitable Zone Search for Life Beyond the Solar System: Exoplanets, Biosignatures & Instruments
Neron de Surgy, O., & Laskar, J. 1997, A&A, 318, 975
Ohta, Y., Taruya, A., & Suto, Y. 2009, ApJ, 690, 1
Petigura, E. A., Howard, A. W., & Marcy, G. W. 2013, PNAS, 110, 19273
Pierrehumbert, R., & Gaidos, E. 2011, ApJL, 734, L13
Rappaport, S., Levine, A., Chiang, E., et al. 2012, ApJ, 752, 1
Ricker, G. R. 2014, The Transiting Exoplanet Survey Satellite Mission, Search for Life Beyond the Solar System: Exoplanets, Biosignatures & Instruments
Ricker, G. R., Winn, J. N., Vanderspek, R., et al. 2014, SPIE J. Ast. Tel. Inst. & Sys., in press (arxiv:1406.0151)
Rowe, J. F., Bryson, S. T., Marcy, G. W., et al. 2014, ApJ, 784, 45
Sagan, C., & Drake, F. 1975, SciAm, 232, 80
Scalo, J., Kaltenegger, L., Segura, A. G., et al. 2007, AsBio, 7, 85
Shkolnik, E., & Barman, T. 2014, HAZMAT I: The Evolution of X-ray Far-UV and Near-UV Emission from Early M Stars, Search for Life Beyond the Solar System: Exoplanets, Biosignatures & Instruments
Tarter, J. 2001, ARA&A, 39, 511
Tarter, J. C., Backus, P. R., Mancinelli, R. L., et al. 2007, AsBio, 7, 30
Tian, F. 2014, Stability and Oxygen Contents of the Atmospheres of Planets in the HZ of M dwarfs,Search for Life Beyond the Solar System: Exoplanets, Biosignatures & Instruments
Tusnski, L. R. M., & Valio, A. 2011, ApJ, 743, 97
Van Cleve, J. E., & Caldwell, D. A. 2009, *Kepler* Instrument Handbook (KSCI-19033), (Moffet Field, CA: NASA Ames Research Center)
Von Korff, J., Demorest, P., Heien, E., et al. 2013, ApJ, 767, 40
Weiss, L. M., & Marcy, G. W. 2014, ApJL, 783, L6
Wright, J. L. 1992, Space Sailing (Philadelphia, PA: Gordon and Breach)
Wright, J. T., Fakhouri, O., Marcy, G. W., et al. 2011, PASP, 123, 412
Wright, J. T., Griffith, R. L., Sigurdsson, S., Povich, M. S., & Mullan, B. 2014a, ApJ, 792, 27
Wright, J. T., Mullan, B., Sigurdsson, S., & Povich, M. S. 2014b, ApJ, 792, 26
Zombeck, M. V. 1990, in Handbook of Space Astronomy and Astrophysics (2nd ed.; Cambridge: Cambridge Univ. Press), 72
Zsom, A., Seager, S., de Wit, J., & Stamenković, V. 2013, ApJ, 778, 109
Zuluaga, J. I., Bustamante, S., Cuartas, P. A., & Hoyos, J. H. 2013, ApJ, 770, 23